Review of Scientific Instruments

Symmetric and asymmetric shocked gas jets for laser-plasma experiments

Cite as: Rev. Sci. Instrum. **92**, 083302 (2021); https://doi.org/10.1063/5.0051173
Submitted: 23 March 2021 • Accepted: 26 July 2021 • Published Online: 09 August 2021

L. Rovige, J. Huijts, A. Vernier, et al.

View Online Export Citation CrossMark

ARTICLES YOU MAY BE INTERESTED IN

Optimization and stabilization of a kilohertz laser-plasma accelerator
Physics of Plasmas **28**, 033105 (2021); https://doi.org/10.1063/5.0040926

Gas density structure of supersonic flows impinged on by thin blades for laser–plasma accelerator targets
Physics of Fluids **32**, 066108 (2020); https://doi.org/10.1063/5.0005888

Characterization of supersonic and subsonic gas targets for laser wakefield electron acceleration experiments
Matter and Radiation at Extremes **4**, 015401 (2019); https://doi.org/10.1063/1.5081509

© 2021 Author(s).

AIP Publishing

Review of Scientific Instruments ARTICLE scitation.org/journal/rsi

Symmetric and asymmetric shocked gas jets for laser-plasma experiments

Cite as: Rev. Sci. Instrum. 92, 083302 (2021); doi: 10.1063/5.0051173
Submitted: 23 March 2021 • Accepted: 26 July 2021 •
Published Online: 9 August 2021

View Online Export Citation CrossMark

L. Rovige,[1,a)] J. Huijts,[1] A. Vernier,[1] I. Andriyash,[1] F. Sylla,[2] V. Tomkus,[3] V. Girdauskas,[3,4] G. Raciukaitis,[3] J. Dudutis,[3] V. Stankevic,[3] P. Gecys,[3] and J. Faure[1]

AFFILIATIONS

[1] Laboratoire d'Optique Appliquée, ENSTA, CNRS, Ecole Polytechnique, Institut Polytechnique de Paris, 828 Bv des Maréchaux, 91762 Palaiseau, France
[2] SourceLAB, 7 rue de la Croix Martre, 91120 Palaiseau, France
[3] Center for Physical Sciences and Technology, Savanoriu Ave. 231, LT-02300 Vilnius, Lithuania
[4] Vytautas Magnus University, K. Donelaicio St. 58, LT-44248 Kaunas, Lithuania

[a)] **Author to whom correspondence should be addressed:** lucas.rovige@ensta-paris.fr

ABSTRACT

Shocks in supersonic flows offer both high density and sharp density gradients that are used, for instance, for gradient injection in laser-plasma accelerators. We report on a parametric study of oblique shocks created by inserting a straight axisymmetric section at the end of a supersonic "de Laval" nozzle. The effect of different parameters, such as the throat diameter and straight section length on the shock position and density, is studied through computational fluid dynamics (CFD) simulations. Experimental characterizations of a shocked nozzle are compared to CFD simulations and found to be in good agreement. We then introduce a newly designed asymmetric shocked gas jet, where the straight section is only present on one lateral side of the nozzle, thus providing a gas profile well adapted for density transition injection. In this case, full-3D fluid simulations and experimental measurements are compared and show excellent agreement.

Published under an exclusive license by AIP Publishing. https://doi.org/10.1063/5.0051173

I. INTRODUCTION

The development of laser-plasma accelerators[1,2] (LPAs) requires efforts not only on the laser-driver part of the system but also on the shaping of the plasma target. It is indeed necessary to tailor the plasma profile in order to gain more control on injection and acceleration mechanisms and obtain high quality particle beams suitable for applications such as femtosecond x-ray beam production,[3–5] particle colliders,[6] electron diffraction,[7,8] or medical applications.[9,10]

In electron acceleration, the gradient injection scheme relying on a sharp downward density transition[11–14] has been used in numerous experiments and has proven very efficient to increase the beam quality and stability. It has been mainly implemented through laser-induced density transition[15,16] and by inserting a thin blade in the outflow of a supersonic gas jet,[17–19] which results in the formation of a shock-front in the gas profile. Two different regimes can be distinguished according to the relative size between the gradient scale length and the plasma wavelength λ_p. If $L_{grad} > \lambda_p$, the injection is due to the reduced wake phase velocity in the density transition region, which facilitates trapping.[11] In the case of a sharp transition, $L_{grad} < \lambda_p$, the plasma wavelength increases abruptly because of the sudden change in plasma density, and some background electrons find themselves trapped in the accelerating phase of the wake.[12,13] The sharp gradient configuration favors injection in the first bucket, which yields shorter electron bunches with narrow energy-spread.

Moreover, gas targets are also relevant for ion acceleration experiments in the collisionless shock acceleration[20] regime and magnetic vortex acceleration[21] regime, which occur in a near-critical plasma. At such high density, the laser beam undergoes a strong absorption and is quickly depleted;[22] therefore, these acceleration schemes require a narrow plasma profile with sharp gradients.

Shocks in supersonic flows have several advantages, making them useful tools to tailor the gas profile in laser-plasma experiments: (i) They can provide high densities with sharp profiles needed in ion acceleration experiments; (ii) this high density can be obtained relatively far from the nozzle, which is especially interesting to reduce damage on the target and increase its durability; and (iii) they enable the production of gas profiles with a downward density transition followed by a plateau of particular interest for the gradient injection scheme.

Published under an exclusive license by AIP Publishing

As mentioned earlier, most of the experiments relying on the gradient injection method use a blade inserted in the flow after the nozzle. The physics of supersonic gas jets impinged by a blade has been recently thoroughly described,[23] and such a design works well with millimetric-scale targets used in experiments with high-power lasers where the Rayleigh length is relatively long and thus where distance and positioning constraints are not too stringent. However, in high-repetition rate laser-plasma accelerators with an energy of only a few millijoules per pulse, it is necessary to focus the laser tightly in order to achieve relativistic intensities. The targets are therefore scaled down to micrometric dimensions, and the laser is focused at around 150 μm from the nozzle. With such small dimensions, inserting a knife-edge in the flow with good precision can prove difficult. Moreover, as LPA technology advances, questions of stability and reproducibility gain importance in the perspective of applications and integrating the shock formation in the design of the nozzle would offer a more compact, robust, and simple solution than the blade technique.

In this paper, we study supersonic shock nozzles of micrometric-dimensions, relying on the formation of oblique shocks due to the sudden change in the flow direction in the final section of the nozzle, with fluid simulations and experimental measurements. A symmetrically shocked design yielding a high on-axis density, with a peaked profile,[24] is thoroughly studied through simulations, which are validated by an experimental measurement. We then propose a newly designed asymmetrically shocked nozzle intended to provide the density downramp followed by a plateau necessary for gradient injection. This design is validated through 3D computational fluid dynamics (CFD) simulations and experimental measurements. We recently showed that this kind of nozzle greatly enhances the long-term stability of kilohertz laser-plasma accelerators.[25]

This paper is organized as follows: In Sec. II, we review some physical principles relevant to the study of supersonic flows and oblique shocks, and a simple geometrical model for the on-axis shock position is proposed. Section III presents the methods used for numerical simulations and experimental measurements. Section IV is devoted to the study of symmetrically shocked jets, first with a comparison between the simulation and measurement and then a study of the influence of different parameters with simulations. In Sec. V, we present the design of the one-sided shock nozzle, with CFD simulation and an experimental measurement. Finally, Sec. VI summarizes the results and concludes this paper.

II. THEORY

A. 1D-isentropic flow

The design of the gas jet used to produce an oblique shock consists in a converging–diverging "*de Laval*" nozzle in which a straight duct has been added at the exit of the gas jet to abruptly change the direction of the flow. The converging section is attached to a constant pressure reservoir, and the nozzle exhaust leads to a vacuum chamber. This geometry results in a Mach number of $M = 1$ at the throat and a supersonic flow in the diverging section of the nozzle. The evolution of the flow in such a nozzle has been thoroughly described with a 1D-isentropic model,[26] and the physics of supersonic nozzles in a context similar to ours has already been studied;[27,28] therefore, we will limit ourselves to recalling the main results of the isentropic expansion model. The flow parameters, namely, the temperature T, the pressure p, and the density ρ, can be expressed according to the Mach number M and their initial value in the reservoir.[26] The coefficient γ is the specific heat ratio of the gas, which is 5/3 for monoatomic gases and 7/5 for diatomic gases. A_t is the cross-sectional area of the nozzle at the throat, and A is the area at the interest point,

$$\frac{A_t}{A} = M\left[1 + \frac{\gamma - 1}{\gamma + 1}(M^2 - 1)\right]^{-\frac{\gamma+1}{2(\gamma-1)}}, \tag{1}$$

$$\frac{T}{T_0} = \left(1 + \frac{\gamma - 1}{2}M^2\right)^{-1}, \tag{2}$$

$$\frac{p}{p_0} = \left(1 + \frac{\gamma - 1}{2}M^2\right)^{-\frac{\gamma}{\gamma-1}}, \tag{3}$$

$$\frac{\rho}{\rho_0} = \left(1 + \frac{\gamma - 1}{2}M^2\right)^{-\frac{1}{\gamma-1}}. \tag{4}$$

It appears that all the physical quantities are determined by the ratio between the area of the nozzle at the throat and the area at the considered point. Equation (1) will be of particular interest for our study as it allows us to determine the Mach number, which is one of the governing factors of the behavior of oblique shocks. Moreover, Eq. (4) shows that the density decreases as the nozzle section (and therefore the Mach number) increases. In a simple supersonic nozzle, the same behavior happens at the exit when the flow expands freely into vacuum, leading to a density that decreases quickly with the distance z and a degraded profile. The use of oblique shocks, as described in Sec. II B, makes it possible to compensate for this expansion in order to obtain high densities further from the nozzle.

It is important to note that this model does not take into account the effects of the boundary layer, i.e., the region near the wall where the flow velocity transitions from 0% to 90% of the center velocity and where the isentropic assumption is not valid.

B. Oblique shock theory and geometric model of on-axis peak density position

A shock in a supersonic flow is characterized by a sudden reduction in the Mach number at a certain position, leading to the compression of the gas in the shocked region. This compression leads to a higher density, which is of interest for a gas target design. When a supersonic flow changes direction abruptly, such as when encountering a wedge with a moderate (we will see later what is moderate in this case) deflection angle θ, it generates an oblique shock-wave originating from the corner of the wedge and at an angle β to the original flow direction. We propose to study the configuration sketched in Fig. 1(a) where a straight duct added at the end of the diverging section of a "de Laval" nozzle induces a shock-front of angle $\beta - \theta$ with the longitudinal axis. The shock-fronts then converge on-axis at a distance z_m from the nozzle exit determined by the shock angle and the length of the straight duct. This configuration yields a peaked gas profile with high density relatively far from the nozzle. The relation between the shock angle β, the deflection

Published under an exclusive license by AIP Publishing

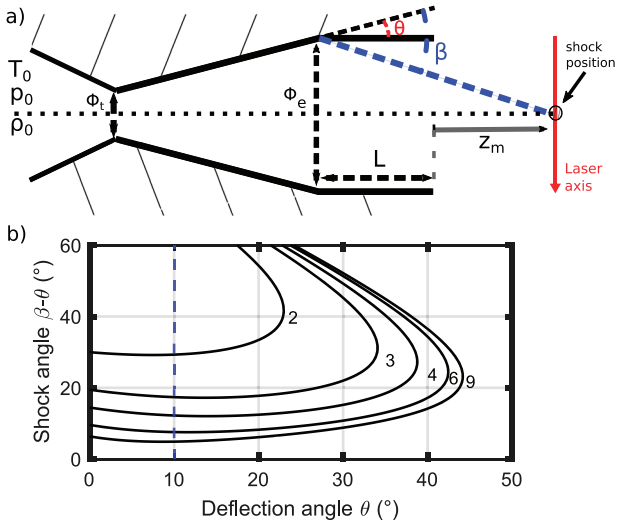

FIG. 1. (a) Schematic description of an oblique shock formation in a shock nozzle. (b) Shock angle as a function of deflection angle for different Mach numbers. The dashed blue line represents the angle of 10° used later in the design of our jets.

angle θ, and the Mach number before the shock M_1 is given by the following equation:[26,29]

$$\tan\,\theta = 2\,\cot\,\beta\,\frac{\mathrm{M}_1^2\sin^2\beta - 1}{\mathrm{M}_1^2\,(\gamma + \cos\,2\beta) + 2}. \tag{5}$$

Equation (5) does not allow us to explicitly express β according to θ and M_1, but we can determine it graphically. The solution of $\beta - \theta$ according to θ for different Mach numbers is displayed in Fig. 1(b). For each deflection angle, there are two solutions: one with a low shock angle, corresponding to the *weak shock* solution, leading to a still supersonic Mach number after the shock $M_2 > 1$, and the other with a higher shock angle, corresponding to the *strong shock* case, with a subsonic downstream flow. Even if no clear mathematical criterion is known, in practice, the *weak shock* case is almost always observed in experiments, as the *strong shock* requires a higher pressure downstream[30] obtained only in specific conditions. In our case where a supersonic flow expands into near-vacuum, the weak shock will therefore occur. Equation (5) does not have any solution for deflection angles $\theta > \theta_{max}$ depending on the Mach number; in this case, the shock solution is not an oblique shock but a detached bow-shock.[26]

It is then possible to determine geometrically the on-axis position of the shock, thanks to the angle $\beta - \theta$,

$$z_m = \frac{\phi_e/2}{\tan(\beta - \theta)} - L, \tag{6}$$

where L is the length of the straight section at the end of the diverging section and ϕ_e is the exit diameter of the nozzle [see Fig. 1(a)]. Even though the oblique shock originates from the corner of the wedge, the on-axis shock position z_m is given with respect to the exit of the nozzle (hence the subtraction of L) because this is the relevant quantity from an experimental point of view.

In order to have a shock position far from the nozzle and preserve its integrity, the shock angle should be kept small. As is clear from Fig. 1(b), this can be obtained through a sufficiently high Mach number (> 3) at the end of the diverging section (determined by A_e/A_t). Although very useful to determine the above principles, this geometrical model does not give indications on the density obtained nor on the effect of the length of the straight section. Numerical simulations are therefore needed to understand these characteristics.

III. METHODS

The simulations are carried out with the CFD software ANSYS Fluent that solves the Navier–Stokes equations. The k-ω shear stress transport (k-ω SST) turbulence model[31,32] is used. It is a robust and efficient model that uses the k-ω formulation near the boundary layers and switches to the k-ϵ formulation in the free-stream. Simulations are performed using nitrogen N_2. Both 2D-axisymmetric and 3D geometries are used depending on the symmetries of the design. The mesh is refined around regions of interest and is composed of ~10^5 cells in the 2D cases and ~5×10^6 cells for the 3D simulations. A convergence study has been performed to ensure that further refining of the mesh does not significantly change the solution. Full-multigrid initialization is used to obtain an initial guess of the solution, thus allowing faster convergence.

For the experimental characterization of the density profile from symmetric and asymmetric nozzles, we use a commercial quadriwave lateral shearing interferometer[33,34] (QWLSI). Here, the gas jet is illuminated by a femtosecond probe laser pulse and imaged onto the CCD camera of the QWLSI using an imaging telescope that consists of a collecting aspherical lens ($f' = 35$ mm) and a lens of focal length $f' = 300$ mm ($f' = 600$ mm) for the symmetric (asymmetric) nozzle case. This imaging system results in resolutions on the QWLSI of 3.2 μm for the symmetric nozzles and 1.9 μm for the asymmetric nozzles, respectively.

The interferometer is based on a Hartmann test combined with a chessboard phase map and works in the following way: The chessboard phase map is inserted in front of the CCD camera and acts as a 2D-diffraction grating that divides the beam into four different waves with different directions of propagation, resulting in a 2D interference pattern. The phase gradients are then retrieved via Fourier analysis, and the phase map is deduced from the integration of these gradients. This interferometer provides a 2D phase map of a 3D object (the gas jet) since the probe laser beam integrates the phase as it propagates through the jet. By assuming the cylindrical symmetry of the object, the 3D density distribution can be retrieved using an Abel inversion algorithm.

Cylindrical symmetry along the z axis is verified for symmetric jets and Abel inversion is used to obtain the molecular gas profile. In this case, the gas jet characterization is performed using molecular nitrogen N_2 because this is the primary gas used in our experiments, and its high refractive index provides a sizable phase shift so that the signal level is high enough for the measurement. The measurement of symmetric nozzles therefore gives access to the complete 3D molecular density distribution $n_{N_2}(r,z)$.

This method cannot be applied to non-axisymmetric jets because the symmetry along z is broken. Instead, the measurement is performed by ionizing the gas with an intense laser pulse: The created plasma column is now approximately axisymmetric along the laser beam propagation axis and Abel inversion can be used again.

Published under an exclusive license by AIP Publishing

Practically, a laser pulse is sent into the gas jet at the desired probing height z_0: The 25 fs, 2 mJ pulses are focused to a 6 μm FWHM spot, therefore reaching an intensity of ~1.3×10^{17} W cm^{-2}, which is one order of magnitude higher than the intensity necessary to ionize nitrogen into N^{5+}. The electron plasma density profile $n_e(r, z_0)$ can then be obtained from the phase map via Abel inversion, assuming radial symmetry around the laser-axis. This is possible under the assumption that the gas density slowly varies over the plasma column radial dimension. Still, the angle between the oblique shock and the normal to the laser propagation axis induces a slight asymmetry in the plasma channel that we neglect. Note that this method gives the density profile for a given height z_0 and needs to be repeated by focusing the intense laser at a different height for exploring the density distribution at different z. Finally, when measuring the plasma profile, the presence of non-ionized gas also affects the measurement of the phase map. We remove the contribution of this residual gas by taking a background phase map without plasma (i.e., the intense laser is turned off) but with gas jet on. This phase image is then subtracted to the plasma phase map in order to remove the contribution from the gas.

IV. SYMMETRIC SHOCKED JETS

When a straight section is added at the end of a "de Laval" nozzle, as pictured in Fig. 1(a), oblique shocks arise from the whole outer diameter of the jet and converge to a point on the axis, resulting in a very dense and narrow gas profile. The study of symmetric shock-jets can be performed in 2D-axisymmetric geometry. This understanding can then be used in the context of the asymmetric shock-jet of Sec. V, which require full-3D simulations.

A. Comparison between measurement and simulation

In order to validate our CFD simulations, we have performed measurements of the gas density profile of a symmetric shock-jet. Figure 2 shows the results of the measurement performed on a jet with ϕ_t = 60 μm, ϕ_e = 180 μm, and a 10° diverging section, with a straight duct length of L = 100 μm, and the comparison with the simulated profile. The isentropic model predicts a Mach number of 3.8 at the end of the diverging section, which would result in a $13° \beta - \theta$ shock angle. The geometric model of Sec. II B predicts an on-axis shock position at $z_{m,th}$ = 289 μm.

The measurement indeed shows the convergence of shock structures on the jet axis, yielding a substantially high density and peaked profile. The simulation prediction of the position of the shock is $z_{m,s}$ = 176 μm, while the measured position is $z_{m,m}$ = 166 μm, which shows a fairly good agreement. These values are significantly lower than predicted by the geometrical model, indicating that the boundary layer plays an important role in the physics of micrometric jets. In the simulation, the center Mach number at the end of the diverging section is 3.6, and the flow velocity decreases near the walls. The simulated and measured gas density transverse profiles at the on-axis shock position are shown in Fig. 2(c). Both profiles have similar widths, but in the experimental case, the peak density is significantly lower. This could be due to an insufficient resolution (the phase resolution is 3.2 μm) combined with the high on-axis noise of the Abel inversion used to retrieve the density from the measured phase. Still, the good overall agreement between the measurement and simulation validates the use of CFD simulations for the design and study of shocked gas jets.

B. Parametric study

We numerically study the influence of two parameters, the length of the final straight duct L and the diameter of the throat ϕ_t, on the position z_{max} where the shock structures meet on the axis, thus forming a peaked density profile, and on the density n_{max} at this position. The exit diameter is fixed at 300 μm, the angle of the diverging section is fixed at 10°, and the origin of the z axis is the exit of the nozzle.

A numerical study of the effect of the straight duct length, in Fig. 3, is of particular interest, as no information on the matter is given by the theoretical model. In Fig. 3, it appears that for L < 100 μm, an increase in the length of the straight section leads to the shock being formed closer to the nozzle, with a slope of −2.5. For higher values of L, a further increase in the straight duct length has almost no significant effect on the position of the shock other than the nozzle's exit being brought closer to it due to the length increase. On the other hand, the maximum density increases with L until it saturates at L = 150 μm. These results show that a compromise on the final duct length has to be made to obtain high density sufficiently far away from the nozzle to prevent from damaging. In our configuration, values of L larger than 150 μm do not provide any benefit.

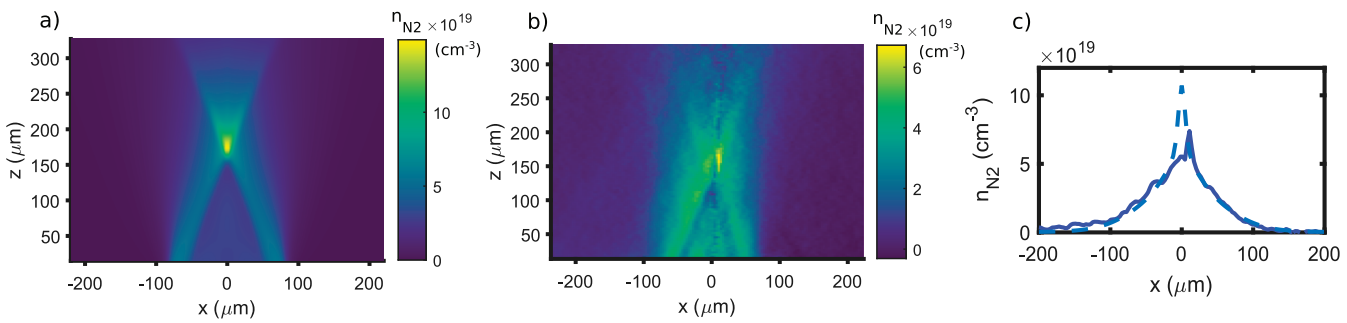

FIG. 2. (a) Simulated and (b) experimental nitrogen molecular density map of a symmetric shock nozzle with a backing pressure of P_{back} = 50 bars. (c) Comparison of the simulated (dashed) and measured (solid) density profiles at $z = z_m$.

Published under an exclusive license by AIP Publishing

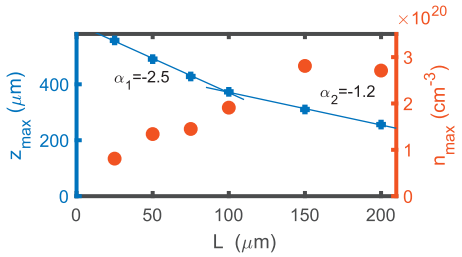

FIG. 3. Simulated on-axis shock position (blue cross) and linear fit for the two regimes, nitrogen molecular density at this position (orange dots), as a function of the length of the final straight duct L. α_1 and α_2 are the slopes of the linear fits. The throat diameter is fixed at $\phi_t = 100\ \mu$m. Simulations are performed in nitrogen with a backing pressure of $P_{back} = 50$ bars.

The influence of L on the shock can be explained by the fact that in the nozzle, the flow direction is not homogeneous. On the center of the nozzle, the gas flows parallel to the axis, while near the walls the flow lines have a 10° angle corresponding to the expansion angle of the nozzle. In the case where L is very short, only the outer flow lines will contribute to the shock because the inner ones will not "see" the change in direction. However, if L is increased, more flow lines will coalesce into the shock-front, which will therefore be stronger. Moreover, the effective deflection angle for these supplementary flow lines is smaller, which results in a larger shock angle (see Fig. 1), which could explain the decrease in z_m with L observed in Fig. 3.

Figure 4 shows the numerical evolution of those two same quantities, shock position and maximum density, as well as the prediction of the geometric model of Sec. II B for the shock position, as a function of throat diameter, with the same geometry as before and a fixed value of L = 100 μm. Reducing the throat diameter while keeping the same exit diameter leads to an increase in the Mach number, as can be deduced from Eq. (1), which can be interesting

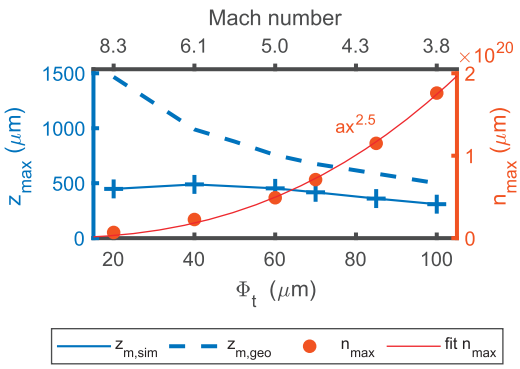

FIG. 4. Evolution of the on-axis shock position (blue cross) and of the maximum density at this point (orange dot) as a function of throat diameter, and the corresponding Mach number at the end of the diverging section. The blue dashed line represents the predictions of the geometrical model of Sec. II. The orange line is a power fit of the maximum density data. Simulations are performed in nitrogen with a backing pressure of $P_{back} = 50$ bars.

in order to increase the distance of the density peak z_m. It appears that the simple geometric model correctly predicts the tendency, despite an offset, of an increase in the shock position when the throat diameter ϕ_t decreases for diameters larger than 60 μm. For smaller ϕ_t, the flow is governed by boundary layers, which are not considered in the simple model, and the shock position saturates around $z_{max} = 500\ \mu$m and even decreases for the smallest diameter considered. Moreover, the offset of the geometric model compared to the simulations for the higher ϕ_t values can be explained again by the effect of the boundary layer, which induces a lower Mach number than calculated with the 1D-isentropic model in the region near the walls, therefore increasing the shock angle.

The maximum density increases with the throat diameter, but this process is largely governed by the evident rise of mass flow rate at the throat due to the larger cross section.

This parametric study shows that by modifying the length of the straight section and the throat diameter, it is possible to control the peak density and its distance from the nozzle. However, both nozzle's features have an opposite impact on the flow characteristics; therefore, a compromise corresponding to the experimental requirement has to be found. With a backing pressure $P_{back} = 50$ bars, nitrogen density up to 2.8×10^{20} cm^{-3} at $z_m = 310\,\mu m$ is predicted with this design, which corresponds to a plasma density of $n_e = 2.8 \times 10^{21}$ cm^{-3} $= 1.6\,n_c$ at $\lambda_0 = 800$ nm after ionization of N_2 into N^{5+}. Symmetric shock nozzles therefore make it possible to reach near-critical to over-critical densities without the need to use a high-pressure compressor. Moreover, with a 150 bar backing pressure, which can be obtained directly at the exhaust of commercial gas bottles, a density even three times higher would be achievable.

V. ONE-SIDED SHOCKED JETS

In this section, we present a design using an oblique shock only on one side of the nozzle, with an opening angle of 96° [see Fig. 5(a)] in order to tailor the gas profile for injection in the sharp density downward transition induced by the shock structure. This design is asymmetric, and therefore, 2D-axisymmetric simulations can no longer be used. It is necessary to perform more extensive full-3D CFD simulations.

The manufacture of such small nozzles with asymmetric features has been made possible by the use of the femtosecond laser-assisted selective etching (FLSE) technique.[35,36] Figure 5(b) shows the simulated density map obtained by using nitrogen with a backing pressure of 15 bars. The straight section here shown on the left side was designed to generate an additional shock propagating at an angle with respect to the jet axis. In the simulation, the shock angle is $\beta - \theta \sim 14°$, which is in good agreement with the theory presented in Sec. II that predicts an angle of 13°. The slight difference can be explained by the effects of boundary layers that are not taken into account by the 1D-isentropic model. A shadowgraphic image of the plasma above the one-sided shock-jet is displayed in Fig. 5(c), and the phase map measured with the QWLSI is shown in Fig. 5(d). Figure 6 compares the density profile obtained in the simulations with the one retrieved from the measured phase map in a nitrogen plasma. Fluid simulations give us the N_2 molecular density from which we retrieve the corresponding plasma density by assuming

Published under an exclusive license by AIP Publishing

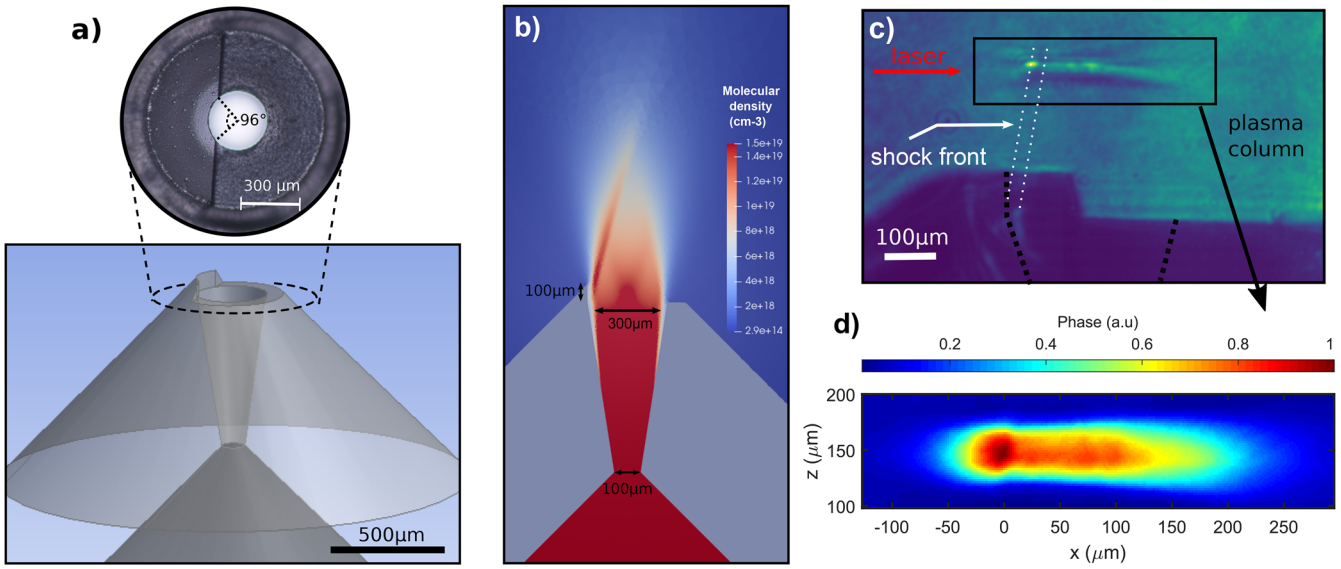

FIG. 5. (a) 3D-model of a one-sided shock nozzle, with a zoom on a top-view picture of the nozzle taken with an optical microscope. (b) Slice of the nitrogen density map from 3D CFD Fluent simulation, with a backing pressure of 15 bars. (c) Experimental shadowgraphic image of the plasma. The black dotted line suggests the inner walls of the nozzle, and the white dotted lines highlight the shock-front. (d) Normalized phase map of the plasma channel obtained by quadriwave lateral shearing interferometry at $z = 150\ \mu$m from the nozzle's exit.

ionization up to N^{5+}. The simulation shows a very good agreement with the measured profile as well as with the absolute density value. At $z = 150\ \mu$m, the measured length of the density downward transition is 16 μm (18 μm in the simulation) for a density drop of 26% (21% in the simulation). At $z = 200\ \mu$m, the measured length of the density downward transition is 26 μm (27 μm in the simulation) for a density drop of 31% (24% in the simulation). This typical shock length corresponds to only a few plasma wavelengths in our high density regime ($\lambda_p \sim 3\ \mu$m at $n_e = 1.4 \times 10^{20}$ cm^{-3}), which is well suited to density gradient injection. It also appears that after $x = 75\ \mu$m, there is a decrease in the measured density that is not predicted by the simulation. It has been verified that this is not due to a decrease in intensity by scanning the relative position of the jet with respect to the laser focus. This could be explained by different factors, such as defects inside the geometry of the nozzle or a slight angle between the laser direction and the normal to the shock structure.

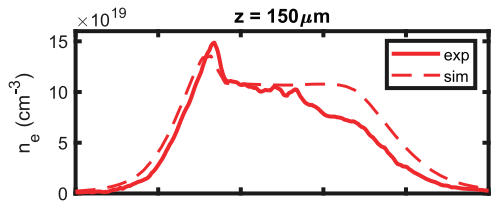

FIG. 6. Comparison of the measured and simulated plasma profile obtained with a one-sided shock nozzle using nitrogen with a backing pressure of 15 bars at a distance of 150 μm.

VI. CONCLUSION

We have presented a CFD-parametric study of the effect of different parameters on the behavior of oblique shock created by a straight section at the end of a supersonic nozzle. Through the modification of the straight duct length and throat diameter, it is possible to control the position and maximum density of the shocked region. We then presented a new design of the shocked gas jet with an oblique shock on only one side, therefore providing a downward density gradient at the beginning of a transverse path in the flow, which can be used for the gradient injection scheme. The knowledge about the behavior of oblique shock obtained through the 2D-axisymmetric simulations of Sec. IV can be applied to the one-sided shock case and provides us with the general laws to modify the characteristics of the density gradient. This new asymmetric design is particularly well suited to small targets where inserting a knife-edge in the flow can be difficult. Because it provides a single-piece solution for shock formation, its robustness and ease-of-implementation can benefit a large number of configurations in laser-plasma experiments. Moreover, the FLSE technique has demonstrated its ability to provide complex asymmetric nozzles with micrometric features and good precision. It could therefore be used to tailor other sophisticated profiles for laser wakefield acceleration, such as controlled density upramp in order to achieve phase locking.[37–39]

ACKNOWLEDGMENTS

We acknowledge Laserlab-Europe under Grant No. H2020 EC-GA 654148 and the Lithuanian Research Council under Grant Agreement No. S-MIP-17-79. This project has received funding from the European Union's Horizon 2020 research and innovation programme under Grant Agreement No. 101004730.

Published under an exclusive license by AIP Publishing

DATA AVAILABILITY

The data that support the findings of this study are available from the corresponding author upon reasonable request.

REFERENCES

[1]T. Tajima and J. M. Dawson, "Laser electron accelerator," Phys. Rev. Lett. **43**, 267–270 (1979).

[2]E. Esarey, C. B. Schroeder, and W. P. Leemans, "Physics of laser-driven plasma-based electron accelerators," Rev. Mod. Phys. **81**, 1229–1285 (2009).

[3]A. Rousse, K. T. Phuoc, R. Shah, A. Pukhov, E. Lefebvre, V. Malka, S. Kiselev, F. Burgy, J.-P. Rousseau, D. Umstadter, and D. Hulin, "Production of a keV x-ray beam from synchrotron radiation in relativistic laser-plasma interaction," Phys. Rev. Lett. **93**, 135005 (2004).

[4]S. Kneip, C. McGuffey, J. L. Martins, S. F. Martins, C. Bellei, V. Chvykov, F. Dollar, R. Fonseca, C. Huntington, G. Kalintchenko, A. Maksimchuk, S. P. D. Mangles, T. Matsuoka, S. R. Nagel, C. A. J. Palmer, J. Schreiber, K. Ta Phuoc, A. G. R. Thomas, V. Yanovsky, L. O. Silva, K. Krushelnick, and Z. Najmudin, Nat. Phys. **6**, 980–983 (2010).

[5]K. Ta Phuoc, S. Corde, C. Thaury, V. Malka, A. Tafzi, J.-P. Goddet, R. C. Shah, S. Sebban, and A. Rousse, "All-optical Compton gamma-ray source," Nat. Photonics **6**, 308–311 (2012).

[6]C. B. Schroeder, E. Esarey, C. G. R. Geddes, C. Benedetti, and W. P. Leemans, "Physics considerations for laser-plasma linear colliders," Phys. Rev. Spec. Top.-Accel. Beams **13**, 101301 (2010).

[7]Z.-H. He, B. Beaurepaire, J. A. Nees, G. Gallé, S. A. Scott, J. R. S. Pérez, M. G. Lagally, K. Krushelnick, A. G. R. Thomas, and J. Faure, "Capturing structural dynamics in crystalline silicon using chirped electrons from a laser wakefield accelerator," Sci. Rep. **6**, 36224 (2016).

[8]J. Faure, B. van der Geer, B. Beaurepaire, G. Gallé, A. Vernier, and A. Lifschitz, "Concept of a laser-plasma-based electron source for sub-10-fs electron diffraction," Phys. Rev. Accel. Beams **19**, 021302 (2016).

[9]O. Rigaud, N. O. Fortunel, P. Vaigot, E. Cadio, M. T. Martin, O. Lundh, J. Faure, C. Rechatin, V. Malka, and Y. A. Gauduel, "Exploring ultrashort high-energy electron-induced damage in human carcinoma cells," Cell Death Dis. **1**, e73 (2010).

[10]O. Lundh, C. Rechatin, J. Faure, A. Ben-Ismaïl, J. Lim, C. De Wagter, W. De Neve, and V. Malka, "Comparison of measured with calculated dose distribution from a 120-MeV electron beam from a laser-plasma accelerator," Med. Phys. **39**, 3501–3508 (2012).

[11]S. Bulanov, N. Naumova, F. Pegoraro, and J. Sakai, "Particle injection into the wave acceleration phase due to nonlinear wake wave breaking," Phys. Rev. E **58**, R5257–R5260 (1998).

[12]P. Tomassini, M. Galimberti, A. Giulietti, D. Giulietti, L. A. Gizzi, L. Labate, and F. Pegoraro, "Production of high-quality electron beams in numerical experiments of laser wakefield acceleration with longitudinal wave breaking," Phys. Rev. Spec. Top.-Accel. Beams **6**, 121301 (2003).

[13]H. Suk, N. Barov, J. B. Rosenzweig, and E. Esarey, "Plasma electron trapping and acceleration in a plasma wake field using a density transition," Phys. Rev. Lett. **86**, 1011–1014 (2001).

[14]J. U. Kim, N. Hafz, and H. Suk, "Electron trapping and acceleration across a parabolic plasma density profile," Phys. Rev. E **69**, 026409 (2004).

[15]T.-Y. Chien, C.-L. Chang, C.-H. Lee, J.-Y. Lin, J. Wang, and S.-Y. Chen, "Spatially localized self-injection of electrons in a self-modulated laser-wakefield accelerator by using a laser-induced transient density ramp," Phys. Rev. Lett. **94**, 115003 (2005).

[16]J. Faure, C. Rechatin, O. Lundh, L. Ammoura, and V. Malka, "Injection and acceleration of quasimonoenergetic relativistic electron beams using density gradients at the edges of a plasma channel," Phys. Plasmas **17**, 083107 (2010).

[17]K. Schmid, A. Buck, C. M. S. Sears, J. M. Mikhailova, R. Tautz, D. Herrmann, M. Geissler, F. Krausz, and L. Veisz, "Density-transition based electron injector for laser driven wakefield accelerators," Phys. Rev. Spec. Top.-Accel. Beams **13**, 091301 (2010).

[18]C. Thaury, E. Guillaume, A. Lifschitz, K. Ta Phuoc, M. Hansson, G. Grittani, J. Gautier, J.-P. Goddet, A. Tafzi, O. Lundh, and V. Malka, "Shock assisted ionization injection in laser-plasma accelerators," Sci. Rep. **5**, 16310 (2015).

[19]K. K. Swanson, H.-E. Tsai, S. K. Barber, R. Lehe, H.-S. Mao, S. Steinke, J. van Tilborg, K. Nakamura, C. G. R. Geddes, C. B. Schroeder, E. Esarey, and W. P. Leemans, "Control of tunable, monoenergetic laser-plasma-accelerated electron beams using a shock-induced density downramp injector," Phys. Rev. Accel. Beams **20**, 051301 (2017).

[20]D. Haberberger, S. Tochitsky, F. Fiuza, C. Gong, R. A. Fonseca, L. O. Silva, W. B. Mori, and C. Joshi, "Collisionless shocks in laser-produced plasma generate monoenergetic high-energy proton beams," Nat. Phys. **8**, 95–99 (2012).

[21]T. Nakamura, S. V. Bulanov, T. Z. Esirkepov, and M. Kando, "High-energy ions from near-critical density plasmas via magnetic vortex acceleration," Phys. Rev. Lett. **105**, 135002 (2010).

[22]F. Sylla, A. Flacco, S. Kahaly, M. Veltcheva, A. Lifschitz, V. Malka, E. d'Humières, I. Andriyash, and V. Tikhonchuk, "Short intense laser pulse collapse in near-critical plasma," Phys. Rev. Lett. **110**, 085001 (2013).

[23]L. Fan-Chiang, H.-S. Mao, H.-E. Tsai, T. Ostermayr, K. K. Swanson, S. K. Barber, S. Steinke, J. van Tilborg, C. G. R. Geddes, and W. P. Leemans, "Gas density structure of supersonic flows impinged on by thin blades for laser–plasma accelerator targets," Phys. Fluids **32**, 066108 (2020).

[24]F. Mollica, "Ultra-intense laser-plasma interaction at near-critical density for ion acceleration," Ph.D. thesis, Université Paris Saclay, 2016.

[25]L. Rovige, J. Huijts, I. Andriyash, A. Vernier, V. Tomkus, V. Girdauskas, G. Raciukaitis, J. Dudutis, V. Stankevic, P. Gecys, M. Ouille, Z. Cheng, R. Lopez-Martens, and J. Faure, "Demonstration of stable long-term operation of a kilohertz laser-plasma accelerator," Phys. Rev. Accel. Beams **23**, 093401 (2020).

[26]R. D. Zucker and O. Biblarz, *Fundamentals of Gas Dynamics* (John Wiley & Sons, 2002).

[27]S. Semushin and V. Malka, "High density gas jet nozzle design for laser target production," Rev. Sci. Instrum. **72**, 2961–2965 (2001).

[28]K. Schmid and L. Veisz, "Supersonic gas jets for laser-plasma experiments," Rev. Sci. Instrum. **83**, 053304 (2012).

[29]H. Liepmann and A. Roshko, *Elements of Gas Dynamics*, Dover Books on Aeronautical Engineering (Dover Publications, 2013).

[30]R. Courant and K. O. Friedrichs, *Supersonic Flow and Shock Waves* (Interscience Publishers, 1948).

[31]D. C. Wilcox *et al.*, *Turbulence Modeling for CFD* (DCW Industries, La Canada, CA, 1998), Vol. 2.

[32]F. R. Menter, "Two-equation eddy-viscosity turbulence models for engineering applications," AIAA J. **32**, 1598–1605 (1994).

[33]J. Primot and L. Sogno, "Achromatic three-wave (or more) lateral shearing interferometer," J. Opt. Soc. Am. A **12**, 2679–2685 (1995).

[34]F. Böhle, M. Kretschmar, A. Jullien, M. Kovacs, M. Miranda, R. Romero, H. Crespo, U. Morgner, P. Simon, R. Lopez-Martens, and T. Nagy, "Compression of CEP-stable multi-mJ laser pulses down to 4 fs in long hollow fibers," Laser Phys. Lett. **11**, 095401 (2014).

[35]A. Marcinkevičius, S. Juodkazis, M. Watanabe, M. Miwa, S. Matsuo, H. Misawa, and J. Nishii, "Femtosecond laser-assisted three-dimensional microfabrication in silica," Opt. Lett. **26**, 277–279 (2001).

[36]V. Tomkus, V. Girdauskas, J. Dudutis, P. Gečys, V. Stankevič, and G. Račiukaitis, "High-density gas capillary nozzles manufactured by hybrid 3D laser machining technique from fused silica," Opt. Express **26**, 27965–27977 (2018).

[37]T. Katsouleas, "Physical mechanisms in the plasma wake-field accelerator," Phys. Rev. A **33**, 2056–2064 (1986).

[38]P. Sprangle, B. Hafizi, J. R. Peñano, R. F. Hubbard, A. Ting, C. I. Moore, D. F. Gordon, A. Zigler, D. Kaganovich, and T. M. Antonsen, "Wakefield generation and GeV acceleration in tapered plasma channels," Phys. Rev. E **63**, 056405 (2001).

[39]E. Guillaume, A. Döpp, C. Thaury, K. Ta Phuoc, A. Lifschitz, G. Grittani, J.-P. Goddet, A. Tafzi, S. W. Chou, L. Veisz, and V. Malka, "Electron rephasing in a laser-wakefield accelerator," Phys. Rev. Lett. **115**, 155002 (2015).

Published under an exclusive license by AIP Publishing